Applied Catalysis B: Environmental 188 (2016) 253–258

Contents lists available at ScienceDirect

Applied Catalysis B: Environmental

journal homepage: www.elsevier.com/locate/apcatb

Photocatalytic oxidation of thiophene on RuO_2/SO_4^{2-}-TiO_2: Insights for cocatalyst and solid-acid

Feng Lin[a,*], Zongxuan Jiang[b], Nanfang Tang[b], Cen Zhang[b], Zhenpan chen[b], Tiefeng Liu[b], Bin Dong[a,*]

[a] Key Laboratory of New Energy and Rare Earth Resource Utilization, State Ethnic Affairs Commission, School of Physics and Materials Engineering, Dalian Nationalities University, Dalian 116600, China
[b] State Key Laboratory of Catalysis, Dalian Institute of Chemical Physics, Chinese Academy of Sciences, 457 Zhongshan Road, Dalian 116023, China

ARTICLE INFO

Article history:
Received 4 December 2015
Received in revised form 1 February 2016
Accepted 4 February 2016
Available online 6 February 2016

Keywords:
Cocatalyst
Solid-acid
Thiophene
Photocatalytic oxidation
RuO_2/SO_4^{2-}-TiO_2

ABSTRACT

Thiophene is one of the main sulfur-containing compounds present in gasoline and difficult to be oxidized with the conventional oxidative processes. Photocatalytic oxidation is believed to be a promising way to remove the sulfur-containing compounds from gasoline. Here we studied the photocatalytic oxidation of thiophene on RuO_2/SO_4^{2-}-TiO_2 photocatalyst. We found that high activity can be achieved on 0.045 wt.% RuO_2/1 M SO_4^{2-}-TiO_2 using molecular oxygen as oxidant. The sulfur in thiophene is oxidized to SO_3 finally. SEM and XRD measurements show that the crystallinity of TiO_2 is greatly improved by sulfation process. IR spectra of pyridine adsorption measurements gives the evidence for that the surface acidity property of TiO_2 is also greatly improved. We can conclude that the synergistic effect of RuO_2 acting as an oxidation cocatalyst and SO_4^{2-}-TiO_2 acting as a Lewis acid which capture superoxide species/activate thiophene molecules is responsible for the activity enchancement of thiophene photocatalytic oxidation. The synergistic effect between oxidation catalysis and acid catalysis is crucial for developing highly active photocatalysts for environmental protection.

1. Introduction

Air pollution, caused by the emission of SO_x, is one of the most serious environmental problems in the world [1], and the automobile exhaust gas is the major source of SO_x formed *via* the burning of sulfur-containing components including thiophene and its derivatives. Sulfur-containing organic compounds are a class of pollutants present in fuel oils and the removal of these pollutants is difficult [2]. Photocatalytic degradation of harmful organic compounds is of great interest and importance for environmental protection [3–7]. It has been demonstrated that many organic pollutants present in water or air stream can be removed by means of photocatalytic oxidation. Several researches have been reported for the photooxidative desulfurization of light oil by TiO_2, Ag-$BiVO_4$ photocatalyst, and photosensitizers together with TiO_2 *etc.* [8–11]. However, the photosensitizer itself is often oxidized and difficult to be recovered from the oxidation systems. Meanwhile, the inertness of thiophene in the oxidative desulfurization is mainly due to the aromaticity and the low electron density on sulfur atom, which makes the oxidation of thiophene molecule more difficult. Therefore, it is ideal to develop an effective photocatalyst for the removal of sulfur-containing compounds in gasoline *via* photocatalytic oxidation.

Thus far, titania-based catalyst as one of the most suitable semiconductor photocatalysts has been extensively investigated. TiO_2 has been extensively used in water treatment and air purification, as well as sterilization [12], sanitation, and remediation applications [13,14]. TiO_2 exhibits high activity and stability and has proven to be an excellent photocatalyst material under UV light exposure [15,16]. The photocatalytic activity of titanium dioxide (TiO_2) varies widely with its phase structure, crystallinity and particle size. It is believed that the phase structure and the composition of titania can significantly affect the photocatalytic activity [17–19]. Various methods have been employed to control the crystal phases of TiO_2 [20–24]. Li et al. [25] investigated the photocatalytic reforming of methanol on Pt/TiO_2-SO_4^{2-} as a model reaction of biomass reforming. Sulfated TiO_2 (TiO_2-SO_4^{2-}) with a tunable surface phase was prepared by calcining commercially available titanium dioxide TiO_2 with deposited sodium sulfate Na_2SO_4 as a modifier. Colon et al. [26] used a sol–gel method to synthesize the sulfated TiO_2. They found that SO_4^{2-} can maintain the anatase phase of TiO_2. However, most research of the sulfated TiO_2 reported in the lit-

* Corresponding authors.
E-mail addresses: dong@dlnu.edu.cn, linfeng@dlnu.edu.cn (B. Dong).

http://dx.doi.org/10.1016/j.apcatb.2016.02.016
0926-3373/

erature were used in the photocatalytic esterification reaction and oxidation of alcohols/pollutants [27–29]. The research on the photocatalytic oxidation of thiophene using sulfated TiO_2 has not been reported so far. On the other hand, it is reported that loading a small amount of noble metals or metal oxides, such as Pt, Ag, NiO, and RuO_2 on TiO_2 [30,31], greatly improves the activity of the photocatalysts [32,33]. Very recently, we have found that the excellent photocatalytic activity of thiophene oxidation by photocatalyst $TiO_2/BiVO_4$ co-loaded with ultra-low loadings of Pt and RuO_2 cocatalysts. Pt and RuO_2, shows the strongly synergistic effect between the two cocatalysts on the photocatalytic activity of thiophene oxidation [34,35].

Herein we studied the sulfated TiO_2 loaded with less than 0.05 wt% loading of RuO_2 (denoted as RuO_2/SO_4^{2-}-TiO_2) used in the photocatalytic oxidation of sulfur-containing organic compound thiophene with molecular oxygen as oxidant under photo irradiation. The crystallinity and surface acidity property of TiO_2 were investigated by SEM, XRD and IR spectra of pyridine adsorption *etc.* measurements. We found that the synergistic effect of RuO_2 acting as an oxidation cocatalyst and SO_4^{2-}-TiO_2 acting as a Lewis acid which capture superoxide species/activate thiophene molecules is beneficial for the efficient photocatalytic oxidation of thiophene. The co-existing oxidation cocatalyst and lewis acid site offers a more promising approach for the photocatalytic oxidation of pollutants.

2. Experimental

2.1. Catalyst preparation

All chemicals used in these experiments were of analytical reagent grade. The RuO_x/SO_4^{2-}-TiO_2 catalysts were prepared by incipient wetness method. TiO_2 (Degussa P25) was submerged in a nM H_2SO_4 solution (n = 0.5, 1, 2, 3). The mixture was sonicated for 5 min. This effectively drove the H_2SO_4 solution into the pore networks, leading to a homogeneous adsorption of SO_4^{2-} on the surface of TiO_2 [25,26,28]. After that, the mixture was stirred at 50 °C to remove water. The resulting solids were sintered at 450 °C for 3 h to obtain the SO_4^{2-}/TiO_2 solid-acid, and the SO_4^{2-}/TiO_2 solid-acid were denoted as n M SO_4^{2-}/TiO_2 (n = 0.5, 1, 2, 3 M H_2SO_4). This solid was then submerged in a $(NH_4)_2RuCl6$ solution, sonicated for 30 min and remove water as above, finally sintered at 400 °C for 0.5 h. Thus the samples RuO_x/SO_4^{2-}-TiO_2 were obtained.

2.2. Catalyst characterization

The prepared samples were characterized by X-ray powder diffraction (XRD) on a Rigaku D/Max-2500/PC powder diffractometer. Each sample was scanned using Cu-Kα radiation with an operating voltage of 40 kV and an operating current of 200 mA. The scan rate of 5°/min was applied to record the patterns in the range of 20–80° at a step of 0.02°.

UV–vis diffuse reflectance spectra (UV–vis DRS) were recorded on a UV–vis spectrophotometer (JASCO V-550) equipped with an integrating sphere. The morphologies and particle sizes were examined by scanning electron microscopy (SEM) equipped with a Quanta 200 FEG scanning electron microscope.

Scanning Electron Microscopy (SEM) and Transmission Electron Microscopy (TEM) were used to examine the particle size and morphology. The SEM and TEM images were respectively obtained on a Quanta 200F microscope (FEI Company) with the accelerating voltage of 0.5–30 kV and a Tecnai G2 Spirit (FEI Company) microscopy with the accelerating voltage of 120 kV. High-resolution Transmission Electron Microscopy (HRTEM) images were obtained on a Tecnai G2 F30 S-Twin (FEI Company) instrument.

Infrared spectra of pyridine adsorption were measured with a resolution of 4 cm^{-1} and 32 scans on a Fourier transform infrared spectrometer (Nicolet NEXUS 470). The experiments were carried out in a special IR cell in conjunction with a water-cooling system and a vacuum system. There are several steps in the experimental procedure. The sample, typically 20 mg, was first pressed into a self-supporting thin wafer (15 mm diameter) and then, it was moved into the sample holder of the IR cell. The wafer in the IR cell was evacuated for 1 h to remove the impurities in the cell, and then the background spectrum of the sample was recorded. After introducing the pyridine vapor for 15 min, the wafer was degassed under vacuum condition at 423 K for 30 min before the spectrum was recorded.

Energy Dispersive X-Ray Fluorescence (ED XRF) was used to test the ruthenium, sulfur and oxygen content on the photocatalyst. The measurements were performed on a laboratory-constructed energy-dispersive X-ray fluorescence spectrometer. The air-cooled side window Rh target X-ray tube of ca. 100 mm nominal focal spot size (XTF 5011/75, Oxford Instruments, USA) supplied by an XLG high-voltage generator (Spellman, USA) was used as the excitation source. The X-ray tube was operated at 45 kV and 700 mA. The X-ray spectra emitted by the sample were collected using a thermoelectrically cooled Si-PIN detector (XR-100CR Amptek, Bedford, MA, USA) with a 145 eV resolution at 5.9 KeV that was coupled to a multichannel analyzer (PX4 Amptek, Bedford, MA, USA). The counting time was 600 s.

UV Raman spectra were recorded on a home-assembled UV Raman spectrograph using a Jobin-Yvon T64000 triplestage spectrograph with a spectral resolution of 2 cm^{-1}. The laser line at 325 nm of an He-Cd laser was used as exciting source with an output of 50 mW. The power of the laser at samples was about 1.0 mW.

2.3. Photocatalytic reaction

The photocatalytic reactions were carried out in a Pyrex reaction cell with air bubbled in a constant flow as oxidant. Photocatalyst was dispersed in acetonitrile solution (Photocatalyst concentration is 1 g L^{-1}) containing thiophene ($[\text{sulfur content}]_{initial}$ = 600 ppm). The suspension was irradiated by a high-pressure mercury lamp(300 W, main wave length 365 nm, 0.22 kW/m^2). The temperature of the reaction solution was maintained at 11 ± 2 °C by a flow of cooling water. And the products and byproducts were analyzed by GC-FPD (Agilent 7890, HP-5 column) after separation of the catalyst from the reaction system by centrifugation.

3. Results and discussion

3.1. Characterization of the photocatalyst

The TiO_2 nanoparticles possess diameters of approximately 20–50 nm (Fig. 1a), and the cocatalyst, RuO_x particles are highly dispersed on the surface of TiO_2 for RuO_x/SO_4^{2-}-TiO_2 (Fig. 1b). RuO_x particles (Fig. 1e and f) loaded on SO_4^{2-}-TiO_2 are mainly in the form of semispherical particles. The typical particle size of RuO_x is estimated to be about 5–10 nm. Fig. 1c and d show the TEM and SEM images for the microstructure of the solid-acid catalyst SO_4^{2-}-TiO_2. The image shows that there is some channel structure in the solid-acid catalyst SO_4^{2-}-TiO_2, and the crystallinity of TiO_2 is greatly improved by sulfation process.

Fig. 2a shows the XRD patterns of TiO_2 (the upper curve) and SO_4^{2-}-TiO_2 (the lower curve). For the sample SO_4^{2-}-TiO_2, characteristic diffraction peaks ascribed to TiO_2 were well preserved, which were located at 16.1°, 21.3°, 21.9°, 23.6°. Meanwhile, characteristic diffraction peaks located at 16.1°, 21.3°, 21.9°, 23.6°, 22.0°, 21.3° and 28.1°, which were all ascribed to $TiOSO_4$. This result indi-

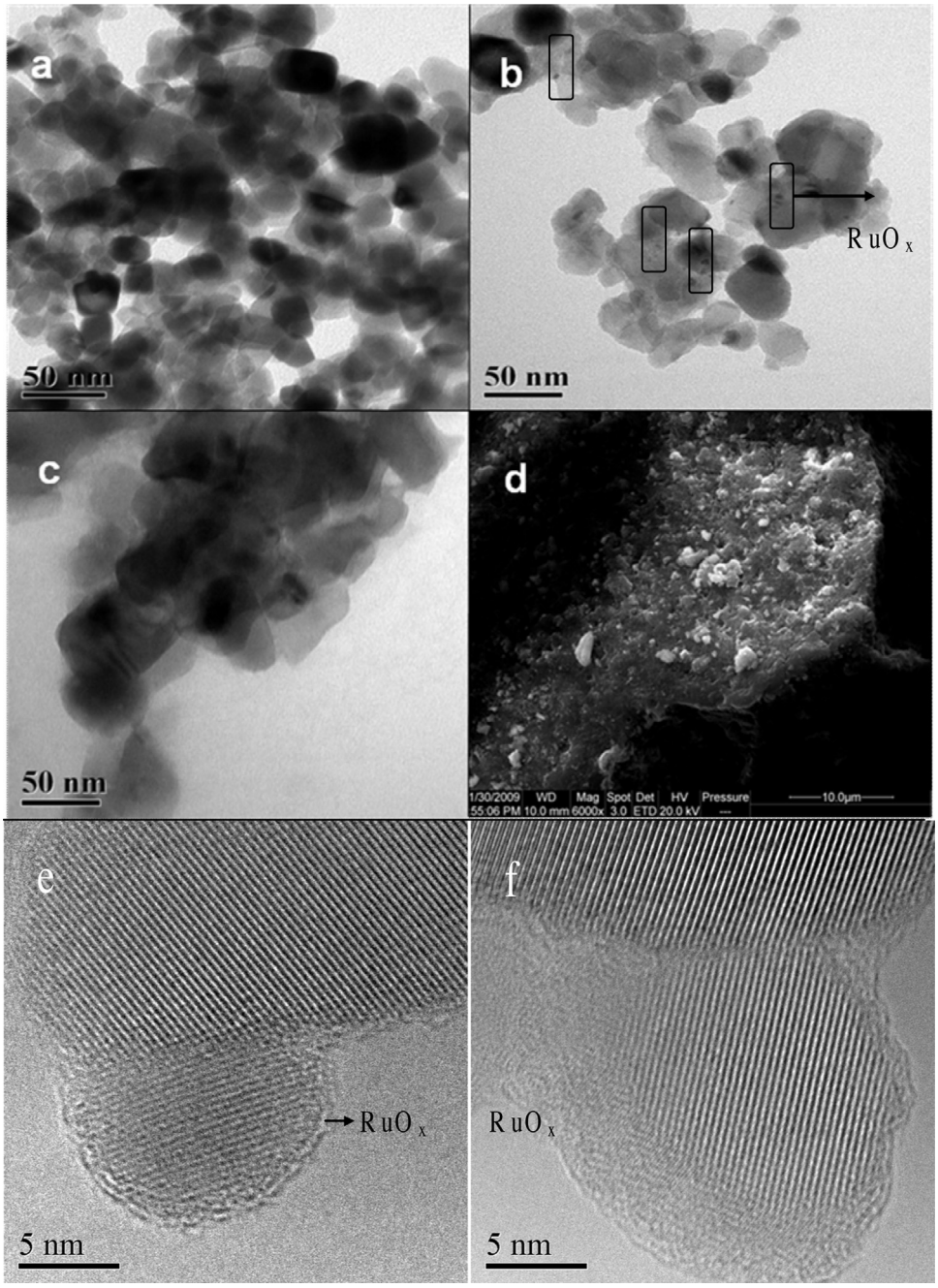

Fig. 1. TEM images of (a) TiO_2, (b) RuO_x/SO_4^{2-}-TiO_2, TEM (c) and SEM (d) images of SO_4^{2-}-TiO_2, (e) and (f) HRTEM images of RuO_x/SO_4^{2-}-TiO_2.

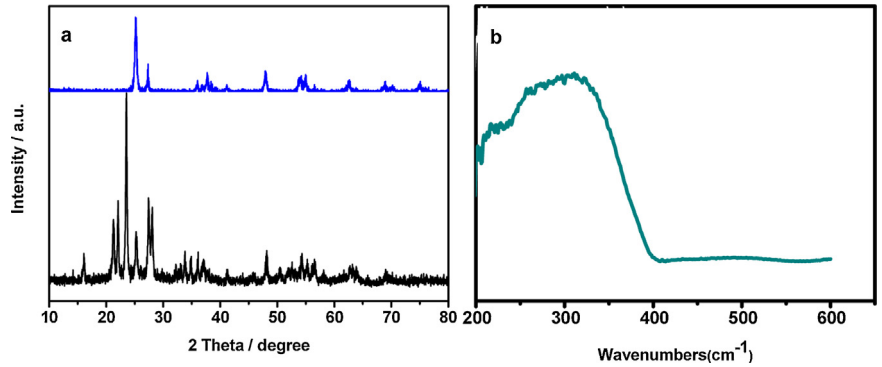

Fig. 2. (a) The XRD patterns of TiO_2 (the upper curve) and SO_4^{2-}-TiO_2 (the lower curve). (b) UV–vis diffuse reflectance spectra of SO_4^{2-}-TiO_2.

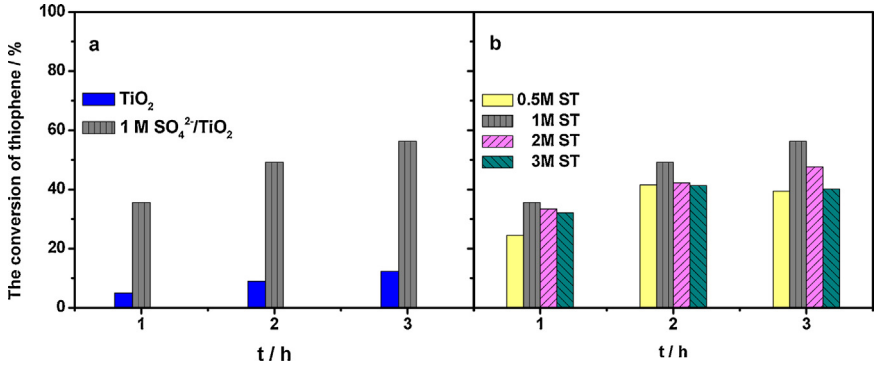

Fig. 3. The photocatalytic activity of thiophene oxidation on various photocatalysts. ST = SO_4^{2-}/TiO_2; Reaction conditions: the concentration of photocatalyst: 1 g L^{-1}; [sulfur content]$_{initial}$ = 600 ppm; light source: High-pressure mercury lamp(300 W, main wave length 365 nm, 0.22 kW/m^2); O_2 (bubbled into the system); temperature: 11 ± 2 °C, reaction time: 3 h.

cates that the phase structure of TiO_2 has been changed by the sulfation process, and $TiOSO_4$ and TiO_2 were existent in the as-prepared SO_4^{2-}-TiO_2 simultaneously. Meanwhile, the diffraction peaks of SO_4^{2-}-TiO_2 are very sharp compared with TiO_2, we can guess that the crystallinity of TiO_2 is greatly improved by sulfation process. Fig. 2b shows the UV–vis diffuse reflectance spectra of SO_4^{2-}-TiO_2. SO_4^{2-}-TiO_2 shows strong absorption in the ultraviolet light region until 410 nm. The band gap of SO_4^{2-}-TiO_2 was estimated to be 2.3 eV from the absorption edge of the UV–vis diffuse reflectance spectrum. There is no obvious shift of the absorption edge between SO_4^{2-}-TiO_2 and TiO_2.

3.2. The effect of acidity on photocatalytic oxidation activity of thiophene

Fig. 3 shows the reaction time courses for thiophene conversion over TiO_2 (Degussa P25), n M SO_4^{2-}/TiO_2 (n = 0.5, 1, 2, 3 M H_2SO_4). As shown in Fig. 3a, TiO_2 (Degussa P25) exhibits very low photocatalytic activity for thiophene oxidation, the conversion of thiophene is only 12.3% for 3 h reaction. The activity is enhanced markedly by sulfation for SO_4^{2-}-TiO_2, and the conversion of thiophene increases to 56.3% for 3 h reaction. As a result, we can conclude that the solid-acid SO_4^{2-}-TiO_2 exhibits superior photocatalytic activity for thiophene oxidation than TiO_2 (Degussa P25). We also studied the dependence of the conversion for photocatalytic oxidation of thiophene on the H_2SO_4 concentration in the synthesis of SO_4^{2-}-TiO_2. As shown in Fig. 3b, as the H_2SO_4 concentration increased from 0.5 to 1 M, the conversion for photocatalytic oxidation of thiophene reaches a maximum, 56.3% when the H_2SO_4 concentration is 1 M. After that, the conversion for photocatalytic oxidation of thiophene on SO_4^{2-}-TiO_2 doesn't increase with the H_2SO_4 concentration. The 3 h conversion for photocatalytic oxidation of thiophene decreases to 47.6% when the H_2SO_4 concentration is 2 M, and lower (*ca.* 40.2%) when 3 M. According to the above results, SO_4^{2-}-TiO_2 is an effective photocatalyst for the photocatalytic oxidation of thiophene compared with TiO_2. The photocatalyst SO_4^{2-}-TiO_2 synthesized with 1 M H_2SO_4 exhibits most superior photocatalytic activity of thiophene oxidation. So 1 M SO_4^{2-}-TiO_2 was synthesized for the following research and photocatalyst preparation.

As shown in the upper discussion, the surface acidity/basicity properties of samples are effective factors for photocatalytic activity of thiophene oxidation. Therefore, the acidities of the samples in our experiments need to be investigated in detail. FT-IR spectroscopy of pyridine adsorption was used to characterize the acidity of the samples. As presented in Fig. 4, five IR peaks are observed in the spectra. Two strong peaks at 1445 cm^{-1} and 1610 cm^{-1} correspond to the coordinated pyridine adsorbed on Lewis acid sites on TiO_2, while the peaks at 1576 cm^{-1} and 1490 cm^{-1} are

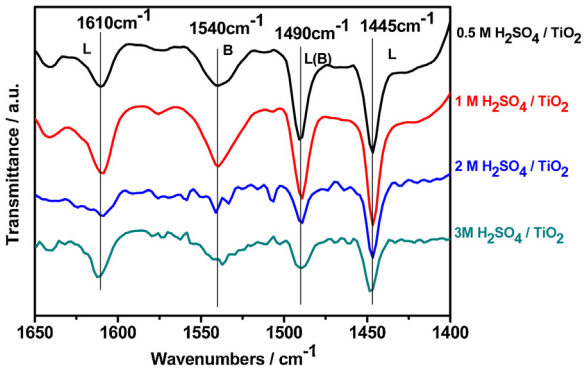

Fig. 4. IR spectra of pyridine adsorption on n M SO_4^{2-}/TiO_2 (n = 0.5, 1, 2, 3 M H_2SO_4).

assigned to the vibrations of pyridine adsorbed on Brønsted acid sites and/or Lewis acid sites on TiO_2 [25]. The characteristic peak at 1540 cm^{-1} corresponds to pyridine adsorbed on Brønsted acid sites on TiO_2. Obviously, the most Brønsted acid sites and/or Lewis acid are detected for 1 M SO_4^{2-}/TiO_2, while the intensities of IR peaks due to pyridine adsorbed on acid sites are sharply decreased for both 2 M SO_4^{2-}/TiO_2 and 3 M SO_4^{2-}/TiO_2. According to the above results, there are similar variation trends between the samples' acidity properties and photocalytic oxidation activity of thiophene. 1 M SO_4^{2-}/TiO_2 with the most Brønsted acid sites and/or Lewis acid exhibits most superior photocatalytic activity of thiophene oxidation (*ca.* 56.3%). This indicates that the surface acidity property of photocatalyst is critical issue for photocatalytic activity of thiophene oxidation.

3.3. The effect of cocatalyst on photocatalytic oxidation activity of thiophene

Fig. 5 shows the conversion for photocatalytic oxidation of thiophene on TiO_2, 1 M SO_4^{2-}-TiO_2 and x wt.% RuO_x/1 M SO_4^{2-}-TiO_2 photocatalysts (x is the calculation amount of RuO_x loading). As shown in Fig. 5a, TiO_2 alone exhibited low conversion for photocatalytic oxidation of thiophene (*ca.* 12%), and the conversion was enhanced by sulfation for 1 M SO_4^{2-}-TiO_2 (*ca.* 56%). Most interestingly, by loading cocatalyst RuO_x, the conversion can at best be enhanced by about 22%. The dependence of the conversion for photocatalytic oxidation of thiophene on the loadings of RuO_x on 1 M SO_4^{2-}-TiO_2 are shown in Fig. 5b. For x wt.% RuO_x/1 M SO_4^{2-}-TiO_2 catalyst, the conversion can be greatly improved when the loading of RuO_x varied from 0 to 0.05 wt.%. As the loading of RuO_x is increased, the conversion is markedly enhanced to a maximum, over 88% when the loading of RuO_x is only 0.05 wt.%. After that, the

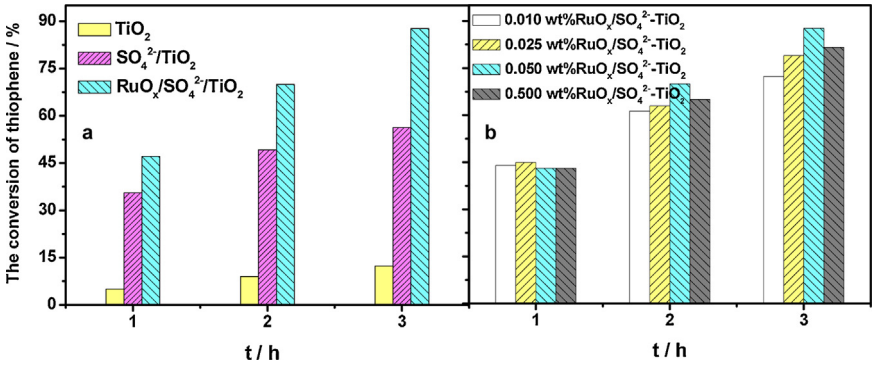

Fig. 5. The photocatalytic activity of thiophene oxidation on various photocatalysts. Reaction conditions: the concentration of photocatalyst: 1 g L^{-1}; [sulfur content]$_{initial}$ = 600 ppm; light source: High-pressure mercury lamp(300 W, main wave length 365 nm, 0.22 kW/m^2); O_2 (bubbled into the system); temperature: 11 ± 2 °C, reaction time: 3 h.

conversion for photocatalytic oxidation of thiophene on RuO_x/1 M SO_4^{2-}-TiO_2 doesn't increase with the loading of RuO_x. The 3 h conversion for photocatalytic oxidation of thiophene decreases to *ca.* 81% when the loading of RuO_x is 0.50 wt.%. It is noteworthy that when only 0.05 wt.% RuO_x was loaded, the conversion can reach as high as 88%. The conversion for photocatalyst with higher loading of RuO_x is not increased obviously, that is, extra amount of RuO_x loaded on SO_4^{2-}-TiO_2 is not necessary. According to the above results, 0.05 wt.% RuO_x/1 M SO_4^{2-}-TiO_2 exhibits most superior photocatalytic oxidation activity of thiophene. The loading of cocatalyst RuO_x greatly improves the photocatalytic oxidation activity of thiophene on the basis of SO_4^{2-}-TiO_2. RuO_x/SO_4^{2-}-TiO_2 is a most effective photocatalyst for the photocatalytic oxidation of thiophene. The synergistic effect of cocatalyst and the surface acidity on TiO_2 could be responsible for the great improvement of photocatalytic oxidation activity of thiophene.

Taking the distinction between experiment and calculation into consideration, Energy Dispersive X-Ray Fluorescence (ED XRF) was used to test the exact ruthenium, sulfur and oxygen content on the 0.05 wt.% RuO_2/1 M SO_4^{2-}-TiO_2 photocatalyst. The results show that ruthenium loaded on the photocalyst surface is 0.0451% (542.644 ppm), and the existence of ruthenium is RuO_2; Sulfur and oxygen content is 8.65% and 44.4% respectively. So the 0.045 wt.% RuO_2/1 M SO_4^{2-}-TiO_2 in fact is the most effective photocatalyst for the photocatalytic oxidation of thiophene in this work.

3.4. The proposed reaction mechanism

Fig. 6 shows the XRD patterns of TiO_2 (Degussa P25) and RuO_2/SO_4^{2-}-TiO_2 before and after the photocatalytic oxidation of thiophene. The XRD patterns show that the anatase and rutile phase in RuO_2/SO_4^{2-}-TiO_2 nearly disappear, and interestingly, we can see that the diffraction peaks attributed to titanyl sulfate (TiOSO4) are much stronger than the anatase and rutile diffraction peaks. The $TiOSO_4$ phase become the main phase structure in RuO_2/SO_4^{2-}-TiO_2. Clearly, the TiO_2 phase structure can be tuned by the sulfation process. After the photocatalytic oxidation of thiophene, the intensity of $TiOSO_4$ phase becomes very weak in the XRD patterns, and there is no obvious change for the anatase and rutile phase. These results indicate that the $TiOSO_4$ phase is the main phase structure in RuO_2/SO_4^{2-}-TiO_2, meanwhile, it could play an important role for the photocatalytic oxidation reaction of thiophene. It should be noted that the stabilization of different phase structure in RuO_2/SO_4^{2-}-TiO_2 decrease in the order: anatase ~ rutile phase > $TiOSO_4$. In previous discussion, the photocatalytic oxidation activities of thiophene show that 0.045 wt.% RuO_2/1 M SO_4^{2-}-TiO_2 is the most effective photocatalyst. The $TiOSO_4$ phase could be probably the active phase for the photocatalytic oxidation reaction of thiophene.

To study the photoproducts, GC-FPD analyzed all of the reaction samples and the air out of outlet was introduced to NaOH

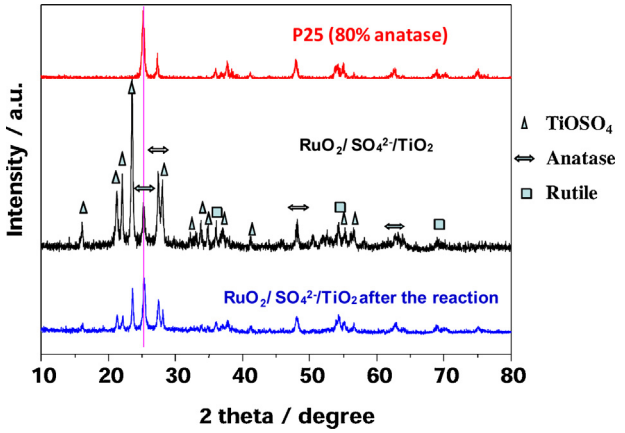

Fig. 6. The XRD patterns of TiO_2 (Degussa P25) and RuO_2/SO_4^{2-}-TiO_2 before and after the photocatalytic oxidation of thiophene.

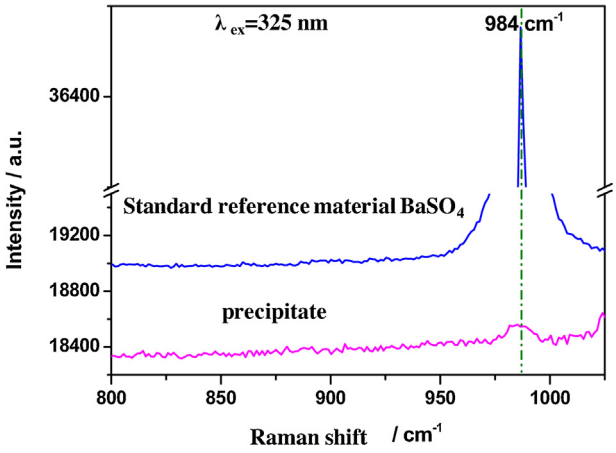

Fig. 7. Raman spectra of the final produced precipitate and standard reference material $BaSO_4$. The gas produced in the reaction system was absorbed by NaOH aqueous solution (0.2 M), then $Ba(NO_3)_2$ (aq) (0.2 M) and HNO_3 (aq) was added successively to produce the final precipitate. Reaction conditions: [sulfur content]initial = 600 ppm; catalyst: RuO_2/SO_4^{2-}-TiO_2; concentration of photocatalyst: 1 g L^{-1}; O_2 (bubbled into the system).

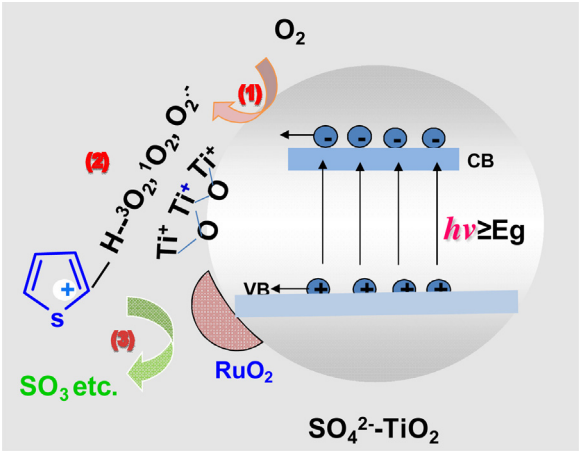

Scheme 1. Schematic description of the mechanism for the photocatalytic oxidation of thiophene on RuO_2/SO_4^{2-}-TiO_2 photocatalyst.

aqueous solution (0.2 M) for the further analysis. After the reaction, a white precipitate was produced when $Ba(NO_3)_2$ aqueous solution (0.2 M) was added into the NaOH (0.2 M) solution. After HNO_3 (aq) we added, there was still some white precipitate existed which could not be dissolved in HNO_3 (aq), and it was denoted as final precipitate. Fig. 7 shows the Raman spectrum (λ_{ex} = 325 nm) of the final precipitate. The Raman bands observed at 984 cm^{-1} is attributed to SO_4^{2-} in $BaSO_4$ [36,37]. The Raman bands of precipitate are in good agreement with those of the standard reference material $BaSO_4$. According to the above results, thiophene can be oxidized to SO_3 in the photocatalytic oxidation system.

A schematic description of the mechanism for the photocatalytic oxidation of thiophene on RuO_2/SO_4^{2-}-TiO_2 is proposed in Scheme 1. The electron-hole can be separated by the cocatalyst loaded on TiO_2 under the illumination. When O_2 is used as the oxidant, photo-generated electron transfer to O_2 on the surface of photocatalyst, where superoxide species $O_2^{\bullet-}$, O_2^{2-} are formed when O_2 reacts with the photo-generated electrons. Thus, the adsorbed oxygen acts as an electron trap, efficiently inhibiting electron-hole recombination [38]. In the given mechanism, SO_4^{2-}-TiO_2 behaves as a typical Lewis acid in the oxidation reaction [29]. It forms an anion radical through an electron acceptor, which can add superoxide species $O_2^{\bullet-}$, O_2^{2-} as shown in Scheme 1. It is believed to be the initiation step in the formation of a very reactive unstable oxidized intermediate formed by addition of the anion radical with thiophene ring in position 2/5 [29,39]. Meanwhile, the photo-generated hole transferred *via* RuO_2 cocatalyst could act as an oxidant [40]. •OH is also generated *via* the reaction of OH^- with hole in the reaction. The interaction of the photo-generated hole and •OH with the reactive oxidized intermediate initiate a series of oxidation reactions. SO_3 is produced finally by the oxidation of sulfur in thiophene. The synergistic effect of RuO_2 acting as an oxidation cocatalyst and SO_4^{2-}-TiO_2 acting as a Lewis acid which capture superoxide species/activate thiophene molecules is beneficial for the efficient transfer of the photo-excited electrons and holes and oxidation of pollutants, being responsible for the high photocatalytic oxidation activity of thiophene.

4. Conclusion

The sulfur-containing organic compound thiophene can be efficiently photocatalyticly oxidized on 0.045 wt.% RuO_2/1 M SO_4^{2-}-TiO_2 using molecular oxygen as oxidant. The sulfur in thiophene can be oxidized to SO_3 finally. SEM, XRD and IR spectra of pyridine adsorption measurements gives the evidence for that the crystallinity and surface acidity property of TiO_2 is greatly improved by sulfation process. We found that the synergistic effect of RuO_2 acting as an oxidation cocatalyst and SO_4^{2-}-TiO_2 acting as a Lewis acid which capture superoxide species/activate thiophene molecules is beneficial for the efficient photocatalytic oxidation of thiophene. The synergistic effect between oxidation catalysis and acid catalysis is crucial for developing highly active photocatalysts for environmental protection.

Acknowledgments

The authors thank Prof. Can Li of Dalian Institute of Chemical Physics (Chinese Academy of Sciences) very much for his great assistance in experiment and discussion. This work was financially supported by the Initial Fund for Imported Talents' Research Project, Dalian Nationalities University (Grants No. 20136126) and Autonomous Research Project, Dalian Nationalities University (Grants No. DC201501072).

Notes and references

References

[1] B. Lee, J. Air Waste Manage. Assoc. 41 (1991) 16–19.
[2] T.V. Choudhary, S. Parrott, B. Johnson, Environ. Sci. Technol. 42 (2008) 1944–1947.
[3] M.R. Hoffmann, S.T. Martin, W.Y. Choi, D.W. Bahnemann, Chem. Rev. 95 (1995) 69–96.
[4] A.L. Linsebigler, G. Lu, J.T. Yates Jr., Chem. Rev. 95 (1995) 735–758.
[5] J. Tang, Z. Zou, J. Ye, Angew. Chem. Int. Ed. 43 (2004) 4463–4466.
[6] D. Chatterjee, S.J. Dasgupta, J. Photochem. Photobiol. C: Photochem. Rev. 6 (2005) 186–205.
[7] H.G. Kim, D.W. Hwang, J.S. Lee, J. Am. Chem. Soc. 126 (2004) 8912–8913.
[8] H.F.M. Zaid, F.K. Chong, M.I.A. Mutalib, Fuel 156 (2015) 54–62.
[9] S. Matsuzawa, J. Tanaka, S. Sato, T. Ibusuki, J. Photochem. Photobiol. A: Chem. 149 (2002) 183–189.
[10] X.M. Gao, F. Fu, L.P. Zhang, W.H. Li, Phys. B: Condens. Matter 419 (2013) 80–85.
[11] Y.J. Yuan, Z.T. Yu, Y.H. Li, H.W. Lu, X. Chen, W.G. Tu, Z.G. Ji, Z.G. Zou, Appl. Catal. B: Environ. 181 (2016) 16–23.
[12] A. Fujishima, T.N. Rao, D.A. Tryk, J. Photochem. Photobiol. C: Photochem. Rev. 1 (2000) 1–21.
[13] A. Fujishima, K. Hashimoto, T. Watanabe, TiO_2 Photocatalysis Fundamentals and Applications, First ed., BKC, Inc., Herndon, VA, 1999, May.
[14] J. Winkler, Macromol. Symp. 187 (2002) 317–324.
[15] M.A. Fox, M.T. Dulay, Chem. Rev. 93 (1993) 341–357.
[16] J. Ryu, W. Choi, Environ. Sci. Technol. 42 (2008) 294–300.
[17] H. Tada, M. Tanaka, Langmuir 13 (1997) 360–364.
[18] Z. Ding, G.Q. Lu, P.F. Greenfield, J. Phys. Chem. B 104 (2000) 4815–4820.
[19] G.H. Li, K.A. Gray, Chem. Phys. 339 (2007) 173–187.
[20] C.M. Ronconi, C. Ribeiro, L.O.S. Bulhoes, E.C. Pereira, J. Alloys Compd. 466 (2008) 435–438.
[21] L.Y. Wang, Y.P. Sun, B.S. Xu, J. Mater. Sci. 43 (2008) 1979–1986.
[22] D.S. Hwang, N.H. Lee, D.Y. Lee, J.S. Song, S.H. Shin, S.J. Kim, Smart Mater. Struct. 15 (2006) 74–80.
[23] A. Testino, I.R. Bellobono, V. Buscaglia, C. Canevali, M. D'Arienzo, S. Polizzi, R. Scotti, F. Morazzoni, J. Am. Chem. Soc. 129 (2007) 3564–3575.
[24] H.P. Xu, Y.P. Sun, J.W. Wang, H.Q. Zhan, X.M. Chen, Rare Metal Mater. Eng. 34 (2005) 1089–1093.
[25] Y. Ma, Q. Xu, X. Zong, D.E. Wang, G.P. Wu, X. Wang, C. Li, Energy Environ. Sci. 5 (2012) 6345–6351.
[26] G. Colon, M.C. Hidalgo, J.A. Navio, Appl. Catal. B 45 (2003) 39–50.
[27] D.S. Muggli, L.F. Ding, Appl. Catal. B: Environ. 32 (2001) 181–194.
[28] H.L. Zhang, H.G. Yu, A.M. Zheng, S.H. Li, W.L. Shen, F. Deng, Environ. Sci. Technol. 42 (2008) 5316–5321.
[29] B. Wang, J.P. Zhu, H.Z. Ma, J. Hazard. Mater. 164 (2009) 256–264.
[30] T. Ishihara, N.S. Baik, N. Ono, J. Photochem. Photobiol. A 167 (2004) 149–157.
[31] J.W. Tang, Z.G. Zou, J.H. Ye, Angew. Chem. Int. Ed. 43 (2004) 4463–4466.
[32] M. Yoshida, A. Yamakata, K. Takanabe, J. Kubota, M. Osawa, K. Domen, J. Am. Chem. Soc. 131 (2009) 13218–13219.
[33] K. Maeda, R. Abe, K. Domen, J. Phys. Chem. C 115 (2011) 3057–3064.
[34] F. Lin, D.E. Wang, Z.X. Jiang, Y. Ma, J. Li, R.G. Li, C. Li, Energy Environ. Sci. 5 (2012) 6400–6406.
[35] F. Lin, Y.N. Zhang, L. Wang, Y.L. Zhang, D.E. Wang, M. Yang, J.H. Yang, B.Y. Zhang, Z.X. Jiang, C. Li, Appl. Catal. B: Environ. 127 (2012) 363–370.
[36] J.T. Kloprogge, D. Wharton, L. Hickey, R.L. Frost, Am. Mineral. 87 (2002) 623–629.
[37] D.L. Bish, A. Livingstone, Mineral. Mag. 44 (1981) 339–343.
[38] J. Robertson, T.J. Bandosz, J. Colloid Interface Sci. 299 (2006) 125–135.
[39] A. Corma, H. Garcia, Chem. Rev. 102 (2002) 3837–3849.
[40] M.A. Fox, A.A. Abdel-wahab, Tetrahedron Lett. 31 (1990) 4533–4536.